Muscle metabolic reprogramming underlies the resistance of liver fatty acid–binding protein (LFABP)-null mice to high-fat feeding–induced decline in exercise capacity

Received for publication, November 12, 2018, and in revised form, August 21, 2019 Published, Papers in Press, August 26, 2019, DOI 10.1074/jbc.RA118.006684

Heli Xu[‡§], Angela M. Gajda[‡§], Yin Xiu Zhou[‡], Cristina Panetta[‡], Zoe Sifnakis[‡], Anam Fatima[‡], Gregory C. Henderson[§¶1], and Judith Storch[‡§2]

From the Departments of [‡]Nutritional Sciences and [¶]Exercise Science and [§]Rutgers Center for Lipid Research, Rutgers University, New Brunswick, New Jersey 08901

Edited by Qi-Qun Tang

Liver fatty acid-binding protein (LFABP) binds long-chain fatty acids with high affinity and is abundantly expressed in the liver and small intestine. Although LFABP is thought to function in intracellular lipid trafficking, studies of LFABP-null (LFABP$^{-/-}$) mice have also indicated a role in regulating systemic energy homeostasis. We and others have reported that LFABP$^{-/-}$ mice become more obese than wildtype (WT) mice upon high-fat feeding. Here, we show that despite increased body weight and fat mass, LFABP$^{-/-}$ mice are protected from a high-fat feeding–induced decline in exercise capacity, displaying an approximate doubling of running distance compared with WT mice. To understand this surprising exercise phenotype, we focused on metabolic alterations in the skeletal muscle due to LFABP ablation. Compared with WT mice, resting skeletal muscle of LFABP$^{-/-}$ mice had higher glycogen and intramuscular triglyceride levels as well as an increased fatty acid oxidation rate and greater mitochondrial enzyme activities, suggesting higher substrate availability and substrate utilization capacity. Dynamic changes in the respiratory exchange ratio during exercise indicated that LFABP$^{-/-}$ mice use more carbohydrate in the beginning of an exercise period and then switch to using lipids preferentially in the later stage. Consistently, LFABP$^{-/-}$ mice exhibited a greater decrease in muscle glycogen stores during exercise and elevated circulating free fatty acid levels postexercise. We conclude that, because LFABP is not expressed in muscle, its ablation appears to promote interorgan signaling that alters muscle substrate levels and metabolism, thereby contributing to the prevention of high-fat feeding–induced skeletal muscle impairment.

Fatty acids (FAs)[3] are important metabolic fuels and signaling molecules that play a critical role in regulating energy homeostasis. As seen in the alarming obesity epidemic, disturbances in lipid homeostasis due to excessive energy intake often induce increased plasma free fatty acid levels and ectopic lipid accumulation in tissues such as liver and skeletal muscle, which in turn contribute to insulin resistance, atherosclerosis, and metabolic syndrome (1, 2). Fatty acid–binding proteins (FABPs) are a family of small cytosolic proteins accommodating fatty acids and other hydrophobic ligands and are thought to be involved in intracellular lipid trafficking. Liver FABP (LFABP; FABP1) is the only FABP abundantly expressed in the liver, whereas in the proximal intestine LFABP is coexpressed with intestinal FABP (IFABP; FABP2) (3). LFABP binds a variety of ligands, including long-chain fatty acids, prostaglandins, heme, lysophosphatidic acid, monoacylglycerols (MGs), bile salts, and certain lipophilic drugs (3–6). Unlike other FABPs, LFABP can bind two fatty acids or MGs (4, 6). Moreover, it has been shown to interact with peroxisome proliferator-activated receptors (PPARs), specifically PPARα and PPARγ (5, 8, 9). Upon activation by micromolar concentrations of FAs and FA analogues, PPARs induce transcription of multiple genes encoding proteins involved in FA metabolism, and dysregulation of PPARs is associated with many metabolic diseases (10, 11). LFABP is thought to promote interaction between PPARs and many natural ligands as well as synthetic agonists of PPARα (fibrates) and PPARγ (thiazolidinediones) commonly used for treating type 2 diabetes (5).

Extensive research has provided evidence for both local and systemic functions of LFABP. In the liver, LFABP has been

This work was supported by NIDDK, National Institutes of Health Grant DK-38389 and funds from the New Jersey Agricultural Experiment Station (to J. S.). The authors declare that they have no conflicts of interest with the contents of this article. The content is solely the responsibility of the authors and does not necessarily represent the official views of the National Institutes of Health.

This article contains Table S1.

[1] Present address: Dept. of Nutrition Science, Purdue University, West Lafayette, IN 47907.

[2] To whom correspondence should be addressed: Dept. of Nutritional Sciences, Rutgers University, New Brunswick, NJ 08901. Tel.: 848-932-1689; Fax: 732-932-6837; E-mail: Storch@sebs.rutgers.edu.

[3] The abbreviations used are: FA, fatty acid; FABP, fatty acid-binding protein; LFABP, liver fatty acid–binding protein; MG, monoacylglycerol; IMTG, intramuscular triglyceride; TG, triglyceride; PPAR, peroxisome proliferator-activated receptor; RER, respiratory exchange ratio; CS, citrate synthase; SDH, succinate dehydrogenase; CCOX, cytochrome *c* oxidase; ASM, acid-soluble metabolite; MHC, myosin heavy chain; *Mb*, myoglobin; *Tnnl*, troponin I slow; *Pgc1*α, peroxisome proliferator-activated receptor γ coactivator 1-α; *Acadl*, long-chain acyl-CoA dehydrogenase; *Cpt1*, carnitine palmitoyltransferase 1; *Mcd*, malonyl-CoA decarboxylase; *Pdhk4*, pyruvate dehydrogenase kinase; *Scd1*, stearoyl-CoA desaturase 1; *Srebp1c*, sterol regulatory element-binding protein 1c; *Bcat*, branched-chain amino acid aminotransferase; *Bckdk*, branched-chain ketoacid dehydrogenase kinase; *Cd36*, cluster of differentiation 36; LXR, liver X receptor; BCAA, branched-chain amino acid; MHO, metabolically healthy obesity; qPCR, quantitative PCR; FFA, free fatty acid; GLUT, glucose transporter; HFS, high-saturated-fat (45 kcal %) diet; FCCP, trifluoromethoxy carbonyl cyanide phenylhydrazone; ANOVA, analysis of variance; VDAC, voltage-dependent anion-selective channel; GAPDH, glyceraldehyde-3-phosphate dehydrogenase; J, C57BL/6J; N, C57BL/6N.

demonstrated *in vitro* and *in vivo* to facilitate hepatic FA uptake and trafficking (12–15) as well as to regulate bile acid and cholesterol metabolism (16, 17). In the intestine, we have reported that LFABP is involved in directing MGs to triglyceride synthesis and FAs to oxidative pathways (18). In addition to such local effects, we and others found that LFABP$^{-/-}$ mice became more obese on high-fat diets than WT mice, with a lower respiratory exchange ratio (RER) (18, 19) but a comparable level of insulin resistance (18, 20), supporting an important role of LFABP in regulating whole-body energy homeostasis.

Despite their obese phenotype, we found that LFABP$^{-/-}$ mice displayed higher levels of spontaneous activity than WT mice (18). In the present studies, we compared exercise tolerance in LFABP$^{-/-}$ *versus* WT mice using a treadmill test. We observed a surprising difference in exercise capacity between the high fat–fed LFABP$^{-/-}$ and WT mice: in contrast to the drastic decrease in exercise capacity in high fat–fed WT mice compared with their low fat–fed littermates, high fat–fed LFABP$^{-/-}$ mice maintain their exercise capacity at the level found under low-fat feeding conditions. Human obesity and diabetes are often associated with poor physical fitness and exercise capacity (21, 22), which in turn limits the absolute intensity and duration of exercise that can be carried out; thus, the potential benefits of regular exercise on insulin sensitivity and cardiovascular health in these patients could be limited. Therefore, an understanding of the physiological alterations in the skeletal muscle of LFABP$^{-/-}$ mice that underlie their resistance to high-fat feeding–induced decline in exercise capacity may provide important information relevant to the maintenance of a healthful exercise capacity in the obese state.

Little has been reported on the effect of LFABP gene knockout on skeletal muscle metabolism, although a microarray analysis indicated higher muscle expression of several genes involved in glucose metabolism and fatty acid oxidation in LFABP$^{-/-}$ mice (23). Given the importance of LFABP in FA metabolism and PPAR signaling, we hypothesized that the deficiency of LFABP and consequent restricted lipid handling capacity in liver, and perhaps intestine, might shunt FAs to extrahepatic tissues, triggering interorgan signaling that would result in metabolic changes in skeletal muscle favoring more efficient energy production. To elucidate how LFABP deficiency increases exercise tolerance under a high-fat feeding regimen, we analyzed substrate availability and energy metabolism in the skeletal muscle of LFABP$^{-/-}$ mice in the resting state and during exercise. The results show that LFABP ablation leads to higher energy substrate levels and mitochondrial respiratory capacity in resting muscles and increased oxidation of circulating FAs during exercise, all of which contribute to preventing the decline in exercise performance that typically accompanies high-fat feeding.

Results

LFABP$^{-/-}$ mice are protected from high-fat feeding–induced decline in exercise capacity

Studies from our laboratory have shown that although there are only modest differences between LFABP$^{-/-}$ and WT mice on low-fat diets, LFABP$^{-/-}$ mice become more obese than WT mice when challenged with high-fat diets (18, 24). Despite the higher weight gain and fat mass, however, they displayed increased spontaneous activity levels (18). Here, we challenged the mice with an exercise tolerance test, and a surprising exercise phenotype in LFABP$^{-/-}$ mice was observed: on low-fat diets, the exercise capacity of WT and LFABP$^{-/-}$ mice was similar. However, in response to high-fat feeding, WT mice showed a marked decrease in exercise capacity, whereas LFABP$^{-/-}$ mice maintained their exercise capacity at a comparable level to their low fat–fed counterparts (Fig. 1, *A* and *B*). Similar results were observed with high fat–fed mice in both fed and fasting states, with LFABP$^{-/-}$ mice showing an approximate doubling of total running distance compared with WT (Fig. 1, *C* and *D*). A side-by-side comparison of two WT and LFABP$^{-/-}$ substrains, one with mixed J/N background and one >98% J, was performed to examine exercise capacity in the fasting state. Compared with the WT mice of the same background, both LFABP$^{-/-}$ strains showed significantly higher exercise capacity, with no differences between the two WT or LFABP$^{-/-}$ BL6 strains (Fig. 1, *E* and *F*). Similarly, no consistent differences in weight gain, fat mass, or food intake were observed between the two substrains (data not shown). Initial observations were first reported in abstract form (25).

High fat–fed LFABP$^{-/-}$ mice have increased muscle substrate availability

To understand how skeletal muscle energy metabolism in LFABP$^{-/-}$ mice supports a higher exercise capacity, we examined the fuel supply in their skeletal muscles following 12 weeks of high-fat feeding. We first measured the locally stored substrates, including muscle glycogen and intramuscular triglyceride (IMTG), in resting skeletal muscle of high fat–fed LFABP$^{-/-}$ mice. Compared with WT mice, LFABP$^{-/-}$ mice had significantly higher levels of both muscle glycogen and IMTG (Fig. 2, *A* and *B*), providing an increased substrate availability for energy production. Oil red O staining of frozen cryosections of gastrocnemius muscle further indicated a higher TG content in LFABP$^{-/-}$ mice, with the overall redder background suggesting even distribution among all muscle fibers (Fig. 2*C*).

As the mice were in the fasting state, we also examined the potential role of gluconeogenesis in contributing to muscle fuel supply. Glycerol tolerance tests showed a delayed increase in blood glucose in response to glycerol injection in LFABP$^{-/-}$ mice relative to WT, but the peak glucose level was higher in LFABP$^{-/-}$ mice (Fig. 2*D*). After adjusting for baseline levels, LFABP$^{-/-}$ mice had a higher area under the curve than the WT mice, suggesting a greater gluconeogenesis capacity (Fig. 2*E*). In contrast, fasting blood glucose and glucose tolerance levels are similar between the genotypes, suggesting a comparable hepatic glucose production (18). Using a metabolomics approach, we found overall similar levels of gluconeogenic substrates; however, the LFABP$^{-/-}$/WT ratios were mostly below 1 with possible decreases in plasma lactate ($p = 0.08$, $q = 0.34$) and liver proline and glycine ($p \approx 0.008$, $q = 0.67$) (Table 1). These results suggest that, despite the enhanced gluconeogenesis capacity in LFABP$^{-/-}$ mice, their gluconeogenesis level in the fasting state appears to be similar to the WT due to restriction in substrate availability.

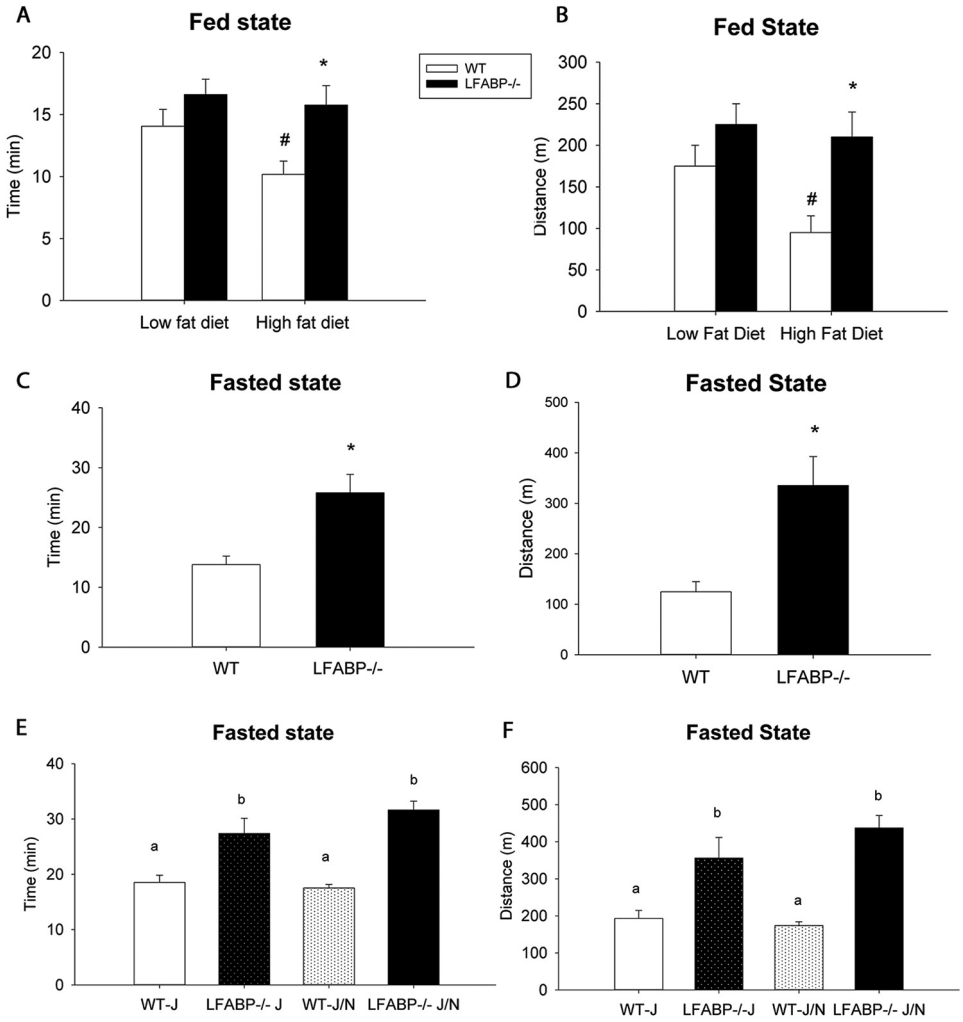

Figure 1. Exercise capacity of low fat– and high fat–fed WT and LFABP$^{-/-}$ mice. Running time and distance until exhaustion point of WT and LFABP$^{-/-}$ mice at 20 weeks of age in fed (*A* and *B*) and fasted (*C* and *D*) states ($n = 8–10$ per group) are shown. *E* and *F*, time and running distance of two strains of WT and LFABP$^{-/-}$ mice in the fasted state ($n = 8–11$). For *A–D*, data are mean ± S.E. (*error bars*), analyzed using Student's *t* test. *, $p < 0.05$ *versus* WT; #, $p < 0.05$ *versus* low-fat diet. For *E* and *F*, data are mean ± S.E. (*error bars*), analyzed using one-way ANOVA with a Tukey's post hoc test. Results with different *letters* are significantly different ($p < 0.05$).

High fat–fed LFABP$^{-/-}$ mice have greater muscle mitochondrial function

Sustained energy is needed to maintain muscle contraction in prolonged exercise, and mitochondrial respiration is the major limiting factor in ATP regeneration (26). Along with the demonstrated increases in glycogen and IMTG availability, we examined mitochondrial function to interrogate the metabolic machinery available to utilize the substrate. Based on the levels of mitochondrial electron transport chain complexes, LFABP$^{-/-}$ mice appear to have a higher mitochondrial quantity in skeletal muscle relative to WT mice (Fig. 3*A*). A marked increase in citrate synthase (CS) activity and a trend toward higher succinate dehydrogenase (SDH) activity in LFABP$^{-/-}$ mice suggest greater mitochondrial function to support substrate utilization in skeletal muscle (Fig. 3, *B* and *C*), although cytochrome *c* oxidase (CCOX) activity was similar in both genotypes (Fig. 3*D*). Furthermore, compared with WT mice, LFABP$^{-/-}$ mice had a higher rate of $^{14}CO_2$ production from [^{14}C]oleic acid in skeletal muscle (Fig. 3*E*), indicating greater capacity for complete fatty acid oxidation. The incomplete fatty acid oxidation levels, considered a measure of insulin sensitivity and mitochondrial overload (27), were similar between LFABP$^{-/-}$ and WT mice, as reflected by the unchanged production rate of acid-soluble metabolite (ASM) (Fig. 3*F*). In addition, mitochondrial respiration was examined with the eahorse system using primary myoblasts isolated from high fat–fed WT and LFBAP$^{-/-}$ mice. Although the basal respiration was similar between the genotypes, LFABP$^{-/-}$ myoblasts showed a greater respiratory capacity compared with WT myoblasts, further supporting the improved mitochondrial function in high fat–fed LFABP$^{-/-}$ mice (Fig. 3, *G* and *H*).

Muscle fiber composition is not altered in skeletal muscle of LFABP$^{-/-}$ mice

To investigate whether the loss of LFABP alters muscle fiber composition in skeletal muscle, we performed real-time quantitative PCR (qPCR) analyses and Western blotting to determine the levels of several markers for type I and type II myofibers in gastrocnemius muscle of LFABP$^{-/-}$ mice. At the mRNA level, there were no significant differences between LFABP$^{-/-}$ and WT mice

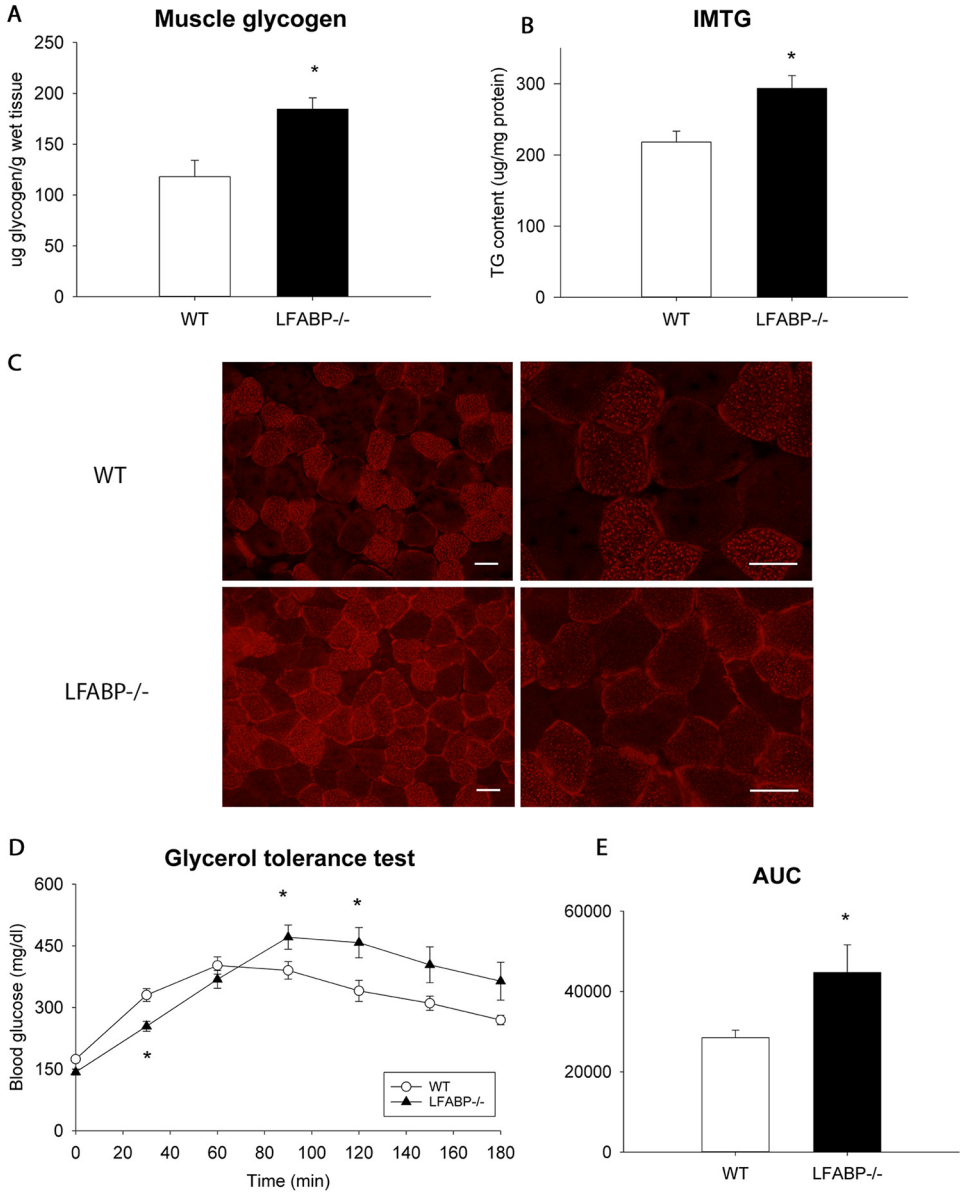

Figure 2. Substrate availability in high fat–fed WT and LFABP$^{-/-}$ mice in the fasted state. Muscle glycogen content ($n = 6–9$ per group) (*A*) and intramuscular triglyceride ($n = 12$ per group) (*B*) are shown. *C*, oil red O staining of frozen cryosections of gastrocnemius muscle (*scale bars*, 50 μm). Blood glucose level (*D*) and area under the curve (*AUC*) (*E*) adjusted for baseline in a glycerol tolerance test in resting mice ($n = 10–12$ per group) are shown. Data are mean ± S.E. (*error bars*), analyzed by Student's *t* test. *, $p < 0.05$ *versus* WT.

in markers for oxidative muscle fibers, including type I–specific myosin heavy chain 1 (*mhc1*), type IIa–specific *mhc2a*, myoglobin (*Mb*), and troponin I slow (*Tnnl*), whereas type IIb–specific *mhc2b* showed a significant decrease in transcriptional level in LFABP$^{-/-}$ mice (Fig. 4*A*). Western blotting confirmed that MHC1 and MHC2a levels were similar between LFABP$^{-/-}$ and WT mice; the decrease in *mhc2b* mRNA levels did not affect its protein abundance in LFABP$^{-/-}$ mice (Fig. 4*B*). Overall, the muscle fiber composition in gastrocnemius muscle appeared unchanged in LFABP$^{-/-}$ relative to WT mice.

LFABP$^{-/-}$ mice show efficient substrate utilization during exercise

As described above, LFABP$^{-/-}$ mice displayed an increased aerobic exercise capacity with a greater mitochondrial function and fatty acid oxidation capacity. Because endurance exercise performance is strongly correlated with aerobic exercise capacity (28), we used indirect calorimetry to examine the substrate utilization of LFABP$^{-/-}$ mice during a 20-min low-intensity (endurance type) exercise. The exercise protocol was designed to allow all mice to complete the test, and the mice were fasted overnight before the test to promote fatty acid utilization and keep the condition consistent with the pre-exercise (resting) analysis. LFABP$^{-/-}$ and WT mice did not exhibit markedly different RER values at any single time point (Fig. 5*A*), but the average RER of the first and second halves of the 20-min exercise bout showed different patterns. In the first 10 min, LFABP$^{-/-}$ mice had a higher average RER than WT mice, suggesting relatively more energy production from carbohydrate utilization; in the second half of the exercise, LFABP$^{-/-}$ mice

Table 1
Glucogenic substrates in the liver and plasma of WT and LFABP$^{-/-}$ mice

Shown is a comparison of metabolite levels measured from samples of the liver and plasma from LFABP$^{-/-}$ mice and WT controls following 12 weeks of high-fat feeding ($n = 5$ per group). Metabolites were determined by LC-MS/MS. *, $p < 0.05$ between WT and LFABP$^{-/-}$; **, $0.05 < p < 0.1$ between WT and LFABP$^{-/-}$.

Metabolites	LFABP-KO/WT ratio	*p* value	*q* value
Glucogenic amino acids in the liver			
Alanine	0.85	0.16	0.70
Aspartate	0.96	0.82	0.72
Asparagine	1.6	0.20	0.70
Glutamate	0.99	0.89	0.73
Glutamine	0.97	0.64	0.71
Cysteine	0.99	0.47	0.70
Proline	0.85*	0.008	0.67
Glycine	0.66*	0.007	0.67
Serine	0.8	0.13	0.70
Threonine	0.87	0.15	0.70
Histidine	0.78	0.16	0.70
Valine	0.93	0.53	0.70
Methionine	0.92	0.33	0.70
Glucogenic and ketogenic amino acids in the liver			
Phenylalanine	0.89	0.13	0.70
Tyrosine	0.89	0.16	0.70
Tryptophan	0.93	0.29	0.70
Isoleucine	0.91	0.26	0.70
Other substrates in the liver			
Glycerol	0.64	0.37	0.70
Lactate	1.11	0.85	0.73
Plasma substrates			
Glycerol	0.99	0.97	0.58
Lactate	0.69**	0.08	0.34

showed a lower average RER compared with WT mice, suggesting a preference for lipid oxidation to provide energy (Fig. 5*B*). Interestingly, although the resting total energy expenditure during 16-h fasting was similar before exercise between the groups (data not shown), LFABP$^{-/-}$ mice displayed a significantly lower energy expenditure during exercise than the WT mice (Fig. 5*C*), even without adjusting for body weights, suggesting that LFABP$^{-/-}$ mice may have better muscle efficiency in energy production than WT mice. In keeping with this, AMP-activated kinase, an important energy sensor in skeletal muscle, was activated in both genotypes in response to the exercise, but the induction level was lower in LFABP$^{-/-}$ mice, suggesting a lower stress response at the cellular level (Fig. 5*D*).

In the skeletal muscle, the decrease in glycogen content during exercise was significantly greater in LFABP$^{-/-}$ mice than in WT (Fig. 4*E*), supporting the higher carbohydrate utilization in the first half of exercise. Postexercise plasma glucose levels were not different between WT and LFABP$^{-/-}$ mice (Fig. 5*G*), suggesting a similar carbohydrate source from the circulation. In terms of muscle lipid utilization, plasma free fatty acid (FFA) levels immediately after exercise were used to examine the FA available for muscle uptake during exercise under the effect of exercise-induced FA release from adipose. Circulating FFA levels were significantly higher in postexercise LFABP$^{-/-}$ mice (Fig. 5*H*), and the decrease in IMTG during exercise was trending lower (Fig. 5*F*), suggesting that the greater FA supply from the plasma contributes to muscle energy production in LFABP$^{-/-}$ mice during exercise.

Differential metabolic regulation and basal metabolites in LFABP$^{-/-}$ muscle

To further define the muscle metabolic changes at the molecular level, we analyzed the expression of several genes involved in lipid and glucose metabolism using qPCR (Fig. 6*A*). The mRNA levels of PPARs were not significantly different in the muscle of LFABP$^{-/-}$ mice compared with WT, although we noted a trend toward a higher level of the PPARα target gene long-chain acyl-CoA dehydrogenase (*Acadl*) in LFABP$^{-/-}$ mice. Interestingly, although the level of cluster of differentiation 36 (*Cd36*) was found to be similar between the genotypes, carnitine palmitoyltransferase 1 (*Cpt1*) and malonyl-CoA decarboxylase (*Mcd*) expression were down-regulated in LFABP$^{-/-}$ mice, suggesting a normal FA uptake into the muscle but a suppression of fatty acid transport into the mitochondria. However, similar levels of *Cs* and *Sdh* mRNA expression between the two groups indicated that the *Cpt1* decrease was not associated with impaired metabolic machinery in LFABP$^{-/-}$ muscles. Because both CS and SDH are encoded by the nuclear genome and synthesized in cytosol before being imported into mitochondria, the increase in CS and SDH activities in LFABP$^{-/-}$ muscle (Fig. 3, *B* and *C*) despite their similar mRNA levels suggests improved mitochondrial protein assembly and overall integrity of the mitochondria. There was no strong evidence suggesting that mitochondrial biogenesis or mitophagy were directly involved in the increased levels of the mitochondrial oxidative phosphorylation complexes (Fig. 3*A*), given the similar mRNA levels of *Pgc1*α (Fig. 6*A*), a major regulator of mitochondrial biogenesis, and similar protein levels of LC3A/B, a mitophagy marker, between the genotypes (data not shown). Both groups had a similar mRNA expression of *fabp3*, the muscle form of FABP, indicating that the ablation of LFABP did not cause any compensatory FABP overexpression in skeletal muscle. Although LFABP$^{-/-}$ mice showed a significant decrease in muscle *glut1* mRNA level (Fig. 6*A*), there was a higher resting GLUT4 abundance on muscle plasma membrane compared with WT (Fig. 6*B*), which may facilitate glucose transport into the skeletal muscle and promote glycogen synthesis. Moreover, LFABP$^{-/-}$ muscle showed similar AKT activation levels in response to insulin injection relative to WT, suggesting an unchanged insulin sensitivity between the two genotypes (Fig. 6*C*).

We also used nontargeted metabolomics to measure alterations in levels of 522 metabolites associated with major metabolic pathways in the skeletal muscle. We found that LFABP$^{-/-}$ muscle had decreased metabolites involved in amino acid signaling (glutamine and asparagine) and specifically in branched-chain amino acid (BCAA) catabolism (β-hydroxyisovaleroylcarnitine, α-hydroxyisovalerate, 2-methylbutyrylcarnitine, and 3-hydroxyisobutyrate) (Table 2). This is consistent with the lower expression levels of BCAA-catabolizing enzymes (*Bcat* and *Bckdk*) in LFABP$^{-/-}$ muscle relative to WT (Fig. 6*D*). In addition, liver X receptor (LXR) signaling was shown to be down-regulated, based on the decreased mRNA of *Lxr*β and its downstream targets, where a trend toward lower *Srebp1c* was noted (Fig. 6*E*).

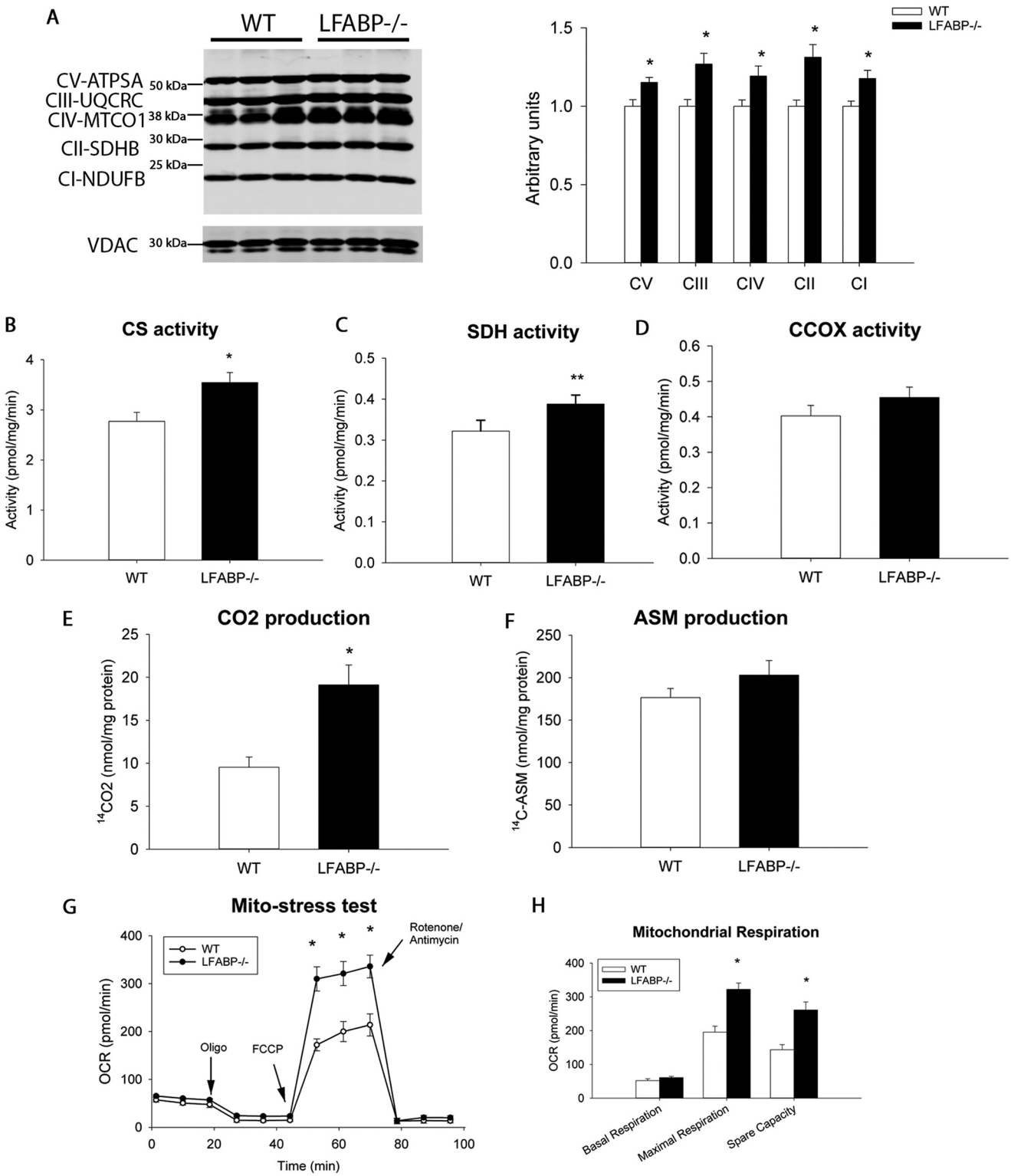

Figure 3. Mitochondrial function in resting skeletal muscles and primary myoblasts of high fat–fed WT and LFABP$^{-/-}$ mice. Mitochondrial content in the muscles (*A*) and mitochondrial enzyme activities of CS (*B*), SDH (*C*), and CCOX (*D*) in WT and LFABP$^{-/-}$ skeletal muscle in the fasted state ($n = 7$–9 per group) are shown. $^{14}CO_2$ production (*E*) and ^{14}C-labeled ASMs (*F*) after [^{14}C]oleic acid administration to muscle homogenates from WT and LFABP$^{-/-}$ mice in the fasted state ($n = 8$–9 per group). Oxygen consumption rate (*OCR*) trace from a mitochondrial stress test on primary myoblasts from high fat–fed WT and LFABP$^{-/-}$ mice in the fed state ($n = 3$–5 per group) (*G*) and their average basal respiration before oligomycin (*Oligo*) injection, maximal respiration after FCCP injection, and the spare capacity, defined by the difference between maximal respiration and basal respiration (*H*) are shown. Oligomycin, ATP inhibitor; FCCP, ionophore that shuttles protons for mitochondrial uncoupling; rotenone/antimycin, complex I and III inhibitors, respectively. Data are mean ± S.E. (*error bars*), analyzed by Student's *t* test. *, $p < 0.05$ *versus* WT; **, $p = 0.07$ *versus* WT. *CI–CV*, complexes I–V.

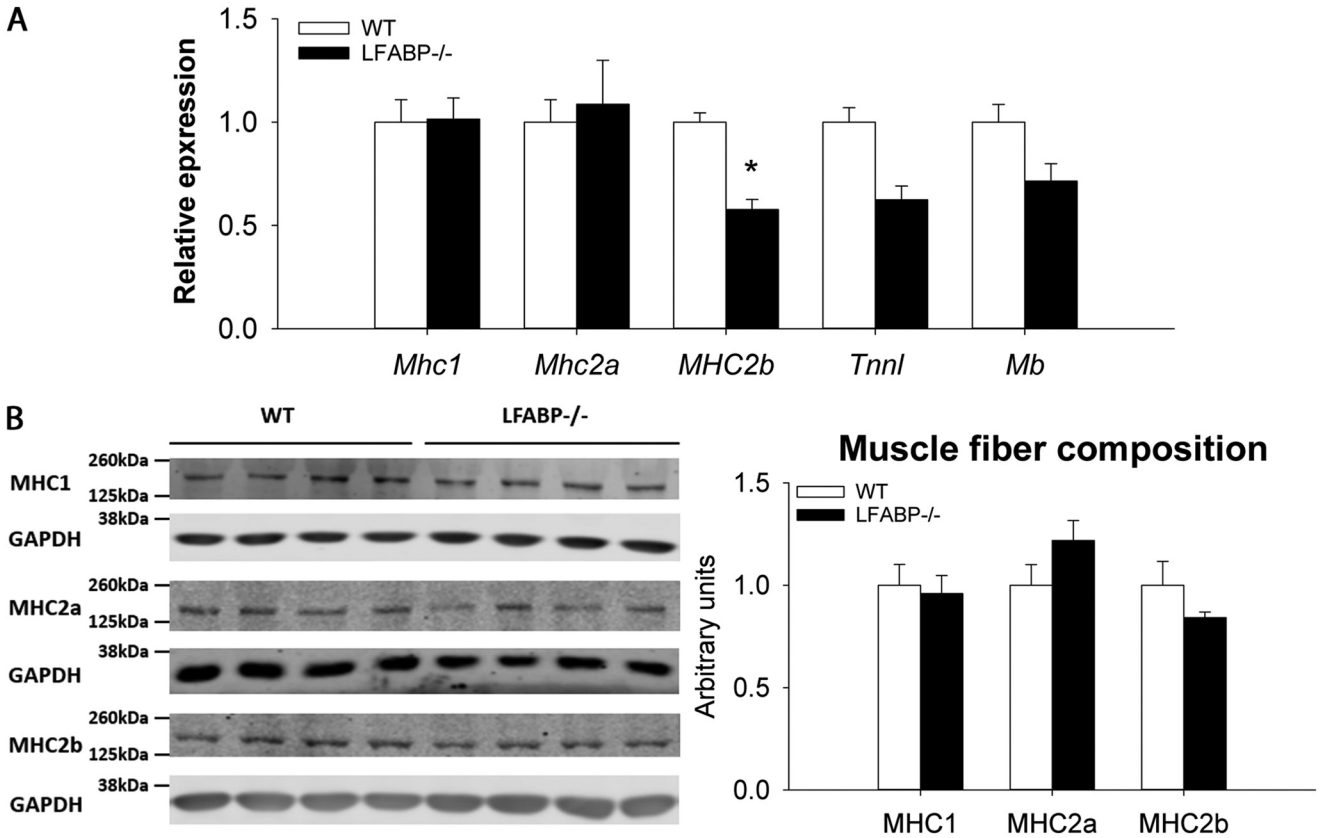

Figure 4. Muscle fiber characterization in gastrocnemius muscle of high fat–fed WT and LFABP$^{-/-}$ mice. Relative quantitation of mRNA expression (*A*) and protein levels (*B*) of markers for different myofibers ($n = 7–8$ per group) are shown. Data are mean ± S.E. (*error bars*), analyzed by Student's *t* test. *, $p < 0.05$ *versus* WT.

Discussion

Exercise capacity is affected by many physiological factors that support sustained energy production for muscle contraction, particularly mitochondrial function and substrate availability (26, 29, 30). As skeletal muscle is one of the major metabolic engines of the body, obesity and associated conditions like metabolic syndrome have been shown to render impaired energy metabolism in skeletal muscle, including decreased glycogen synthesis, excessive oxidative stress, and mitochondrial dysfunction (31–33). Consequently, physical fitness and exercise capacity are generally limited in obese and insulin-resistant individuals (21, 22). Such impaired energy metabolism in skeletal muscle does not seem to be restricted to the obese population because even a short-term high-fat feeding has been shown to induce a significant decrease in exercise capacity without substantial weight gain (34, 35). Although exercise is well-accepted as a major therapeutic intervention for treating obesity and insulin resistance (36, 37), it can be very challenging for patients to follow a recommended exercise regimen due to their low fitness level, impeding the benefits of exercise in managing these metabolic diseases. Indeed, inactivity and poor aerobic fitness have been found to be more important than overweight and obesity as mortality predictors (38, 39).

In this report, we show that LFABP ablation, when accompanied by lipid overload caused by chronic high-fat feeding, is associated with major metabolic alterations in skeletal muscle. These alterations protect LFABP$^{-/-}$ mice from the high-fat feeding–induced decline in exercise capacity. It is worth noting that although LFABP$^{-/-}$ mice showed a higher spontaneous activity level than WT mice, the amount of activity was not enough to increase the total energy expenditure, and therefore "training effects" did not seem to contribute to the exercise phenotype. We previously reported similar glucose tolerance and blood lipid profiles in resting LFABP$^{-/-}$ mice despite their higher adiposity (18). Given the exercise phenotype and improved energy metabolism in skeletal muscle shown here, LFABP$^{-/-}$ mice seem to display signs of metabolically healthy obesity (MHO). MHO is characterized by the absence or alleviation of metabolic abnormalities such as dyslipidemia, insulin resistance, hypertension, an unfavorable inflammatory response, and poor physical fitness (40–42). Indeed, a preliminary study shows that LFABP$^{-/-}$ mice have a longer lifespan compared with WT mice on a chow diet (data not shown), suggesting an improved overall health status of LFABP$^{-/-}$ mice. Notably, as a growing body of evidence has supported the reversible transition between MHO and metabolically unhealthy obesity (43, 44), MHO is recognized as a dynamic status that needs long-term management for sustainable MHO and prevention of progression to the unhealthy stage (45). Thus, understanding the exercise phenotype in LFABP$^{-/-}$ mice may offer a new perspective on breaking the vicious cycle of physical inactivity and obesity.

Both fuel supply and metabolic machinery are important limiting factors for muscle energy production, and both showed

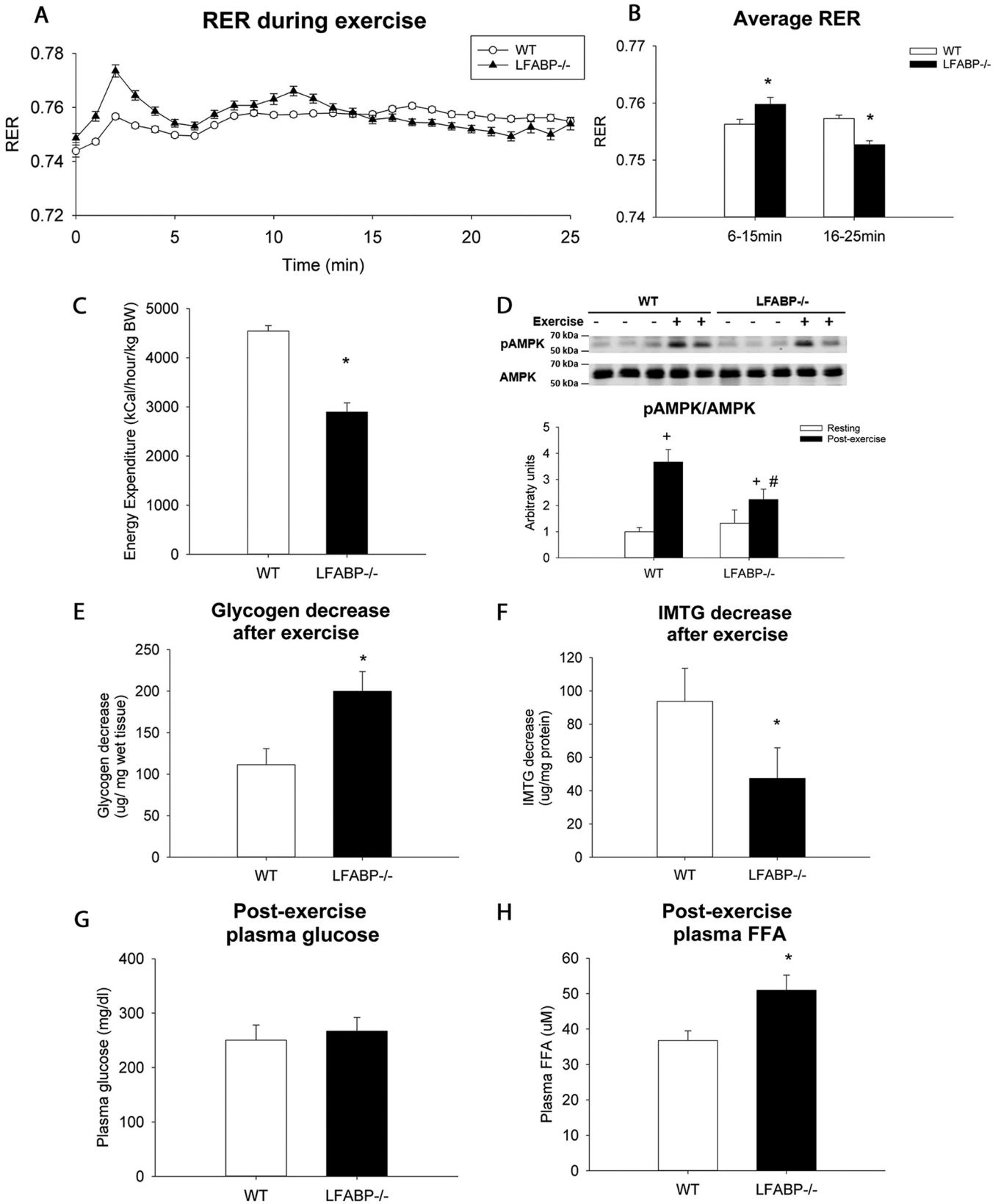

Figure 5. Substrate utilization on the whole-body level and in skeletal muscle of high fat–fed WT and LFABP$^{-/-}$ mice during low-intensity exercise. *A*, RER during a 1-min settlement, 5-min warm-up, and 20-min exercise. *B*, average RER for the first half and second half of the exercise. *C*, energy expenditure during exercise ($n = 8$–10 per group). *D*, AMP-activated kinase (*AMPK*) activation in skeletal muscle in response to exercise ($n = 5$). Muscle glycogen content (*E*) and intramuscular triglyceride (*F*) decreased after exercise ($n = 8$–10 per group). Plasma glucose (*G*) and FFA (*H*) after exercise ($n = 8$–10 per group) are shown. Data are mean ± S.E. (*error bars*), analyzed by Student's *t* test. *, $p < 0.05$ *versus* WT; +, $p < 0.05$ *versus* same genotype in the resting state; # $p \approx 0.05$ *versus* post-exercise WT. *pAMPK*, phosphorylated AMP-activated kinase.

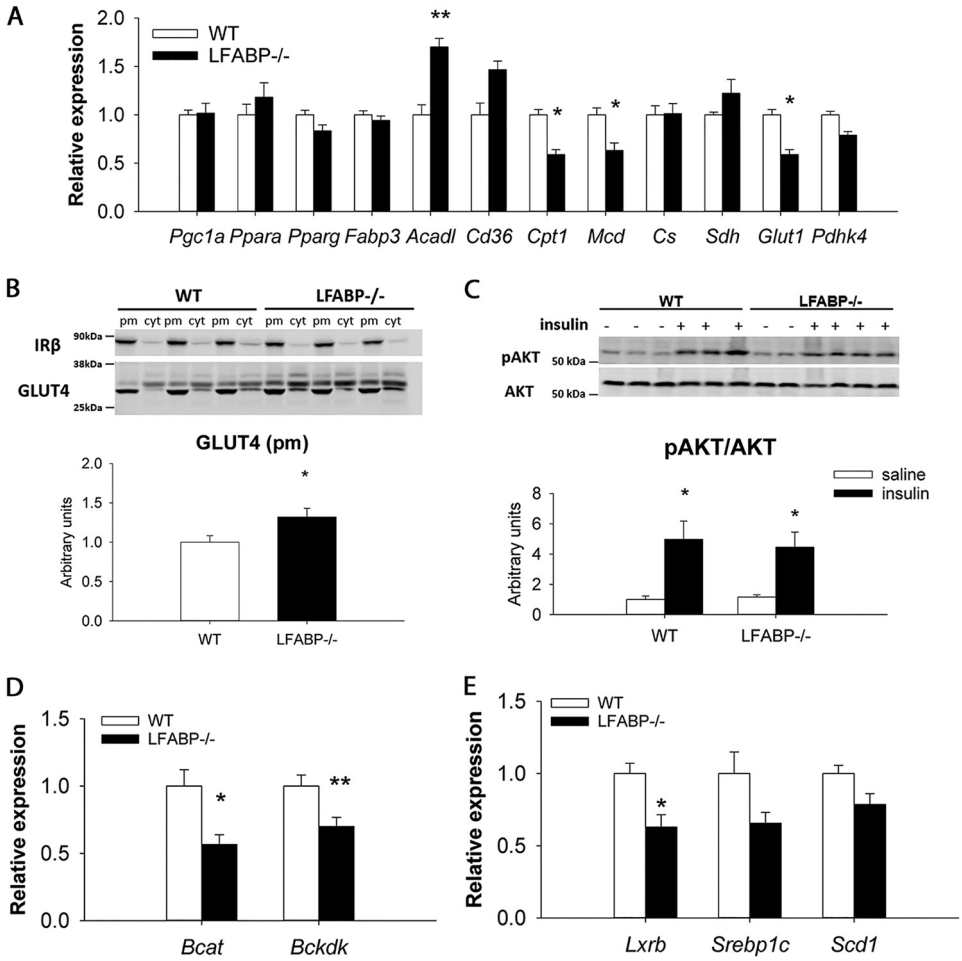

Figure 6. Metabolic regulation in resting muscles of high fat–fed WT and LFABP$^{-/-}$ mice. *A*, mRNA expression levels of genes involved in lipid metabolism and mitochondrial function ($n = 6$–7). *B*, muscle GLUT4 protein abundance on plasma membrane (*pm*) and in cytosol (*cyt*) ($n = 10$). GLUT4 levels on plasma membrane were corrected by the plasma membrane marker insulin receptor β (*IRβ*). *C*, muscle AKT activity in response to insulin injection ($n = 5$–6). *D*, mRNA expression levels of BCAA catabolic genes. *E*, mRNA expression levels of transcription factor LXR and its downstream targets in the skeletal muscle ($n = 6$–7). Data are mean ± S.E. (*error bars*), analyzed by Student's *t*-test. *, $p < 0.05$ *versus* WT; **, $0.05 \leq p \leq 0.07$. *pAKT*, phospho-AKT.

Table 2

Basal metabolites in LFABP$^{-/-}$ and WT muscles

Shown is a comparison of metabolite levels measured from samples of the gastrocnemius muscle isolated from LFABP$^{-/-}$ mice and WT controls following 12 weeks of high-fat feeding ($n = 6$ per group). Metabolites were determined by LC-MS/MS. *, $p < 0.05$ between WT and LFABP$^{-/-}$. AA, amino acid.

Metabolites	LFABP$^{-/-}$/ WT ratio	*p* value	*q* value
AA signaling			
Glutamine	0.83*	0.007	0.21
Asparagine	0.82*	0.004	0.18
BCAA metabolism			
Leucine	0.79	0.18	0.47
4-Methyl-2-oxopentanoate	0.92	0.96	0.73
Isovalerylcarnitine	0.41	0.11	0.47
β-Hydroxyisovaleroylcarnitine	0.63*	0.02	0.30
α-Hydroxyisovalerate	0.53*	0.03	0.33
Isoleucine	0.82	0.23	0.49
allo-Isoleucine	0.55	0.12	0.47
2-Methylbutyrylcarnitine (C5)	0.56*	0.04	0.34
Valine	0.85	0.34	0.53
Isobutyrylcarnitine	0.58	0.23	0.49
3-Hydroxyisobutyrate	0.7*	0.03	0.34

significant changes in high fat–fed LFABP$^{-/-}$ mice, favoring an improved exercise capacity. Although we found that plasma glucose and triglyceride levels were similar between fasting LFABP$^{-/-}$ mice and WT mice, free fatty acids showed a trend toward higher levels in LFABP$^{-/-}$ mice (18). We propose that the increase in IMTG is likely the result of higher FA uptake from the circulation and a decrease in FA β-oxidation as discussed further below and as evidenced by the lower expression levels of two enzymes involved in FA transport into the mitochondria. The marked adiposity, greater intramuscular triglyceride, and possible increase in plasma free fatty acid in LFABP$^{-/-}$ mice also suggest that their inability to process FA in the liver may divert excess FA back to the circulation, leading to FA accumulation, as TG, in other peripheral tissues. The higher muscle glycogen content in LFABP$^{-/-}$ mice does not appear to be secondary to altered insulin sensitivity, as the insulin-responsive cascade regulating glycogen synthase remained unchanged. It is possible that the trend toward higher basal GLUT4 levels at the plasma membrane may promote glucose uptake. Furthermore, a higher GLUT4 expression is also consistent with the observed lower *Glut1* mRNA level in that GLUT1 has been shown to exert a negative feedback effect on GLUT4 activity by directing glucose into the hexosamine pathway (46).

In addition to the greater skeletal muscle substrate availability, high fat–fed LFABP$^{-/-}$ mice exhibit higher mitochondrial

function, as evidenced by the increased mitochondrial quantity, enzyme activities, and fatty acid oxidation capacity. Interestingly, however, the increase in mitochondrial respiratory capacity in LFABP$^{-/-}$ muscle is associated with partial suppression of CPT1 and MCD in the resting state. In contrast to the fatty acid oxidation assays with excess substrate, basal FA β-oxidation depends on mitochondrial FA import (47). CPT1 plays a major role in FA transport into the mitochondria and regulates the rate of β-oxidation; MCD regulates CPT1 activity by degrading its natural inhibitor malonyl-CoA. The down-regulation of both CPT1 and MCD indicates a potential role of decreased basal mitochondrial FA import in preserving mitochondrial function in LFABP$^{-/-}$ muscle under sustained high-FA exposure. Indeed, compared with the WT mice, high fat–fed LFABP$^{-/-}$ mice are at a higher risk of lipid-induced damage to muscle mitochondrial function, with their impaired lipid handling capacity in the liver, trending higher plasma free fatty acids (12, 18, 48), and comparable FA uptake into the muscle cells (similar *Cd36*; Fig. 6*A*). Such lipid overload and a potential for excessive β-oxidation in mitochondria may cause accumulation of FA derivatives as well as reactive oxygen species that interfere with insulin sensitivity and the inflammatory response (for a review, see Martins *et al*. (49)). Thus, the partial suppression in mitochondrial FA import and basal β-oxidation may serve as a brake to the chronic overproduction of lipid intermediates, thereby preserving mitochondrial function in LFABP$^{-/-}$ muscle. This idea agrees with several reports showing that restricted β-oxidation prevents the mitochondrial dysfunction induced by overnutrition. For example, MCD-knockout mice, a genetic model for partial CPT1 inhibition, were protected from the diet-induced glucose intolerance and depletion of tricarboxylic acid cycle intermediates in the skeletal muscle, indicative of compromised mitochondrial status (27). Moreover, pharmacological inhibition of CPT1 corrected the insulin resistance in mice with muscle-specific PPARα overexpression, where lipid-oxidative genes were genetically up-regulated (50). In contrast, PPARα-null mice showed diminished FA oxidation and remained insulin-sensitive under high-fat diets (51).

The finding of similar insulin sensitivity between LFABP$^{-/-}$ and WT muscle is consistent with other evidence showing that a restricted basal FA oxidation and higher mitochondrial function do not always translate into improved insulin sensitivity. For example, inhibiting MCD activity in isolated human skeletal myocytes resulted in decreased FA oxidation and increased glucose uptake but no difference in insulin signaling levels (52). Furthermore, mice with muscle-specific PGC1α overexpression were more prone to diet-induced insulin resistance despite the significant increase in mitochondrial density (53). Thus, the relationship between mitochondrial function and insulin sensitivity is still inconclusive, with numerous reports suggesting all possible scenarios: decreased, unchanged, or increased (compensatory mechanism) mitochondrial function with insulin resistance (for a review, see Montgomery and Turner (54)).

The "crossover" concept for substrate utilization during exercise indicates that relative oxidation of lipid *versus* carbohydrate depends on the exercise intensity relative to the maximal oxygen consumption or aerobic exercise capacity (55). During low-intensity endurance exercise, lipids are the predominant fuel source, and peripheral lipolysis is highly stimulated for FA uptake into muscle, whereas IMTG lipolysis is only stimulated at higher exercise intensity. With increasing exercise intensity, there is a shift toward greater carbohydrate metabolism where plasma glucose uptake and muscle glycogen breakdown are increased (55, 56). During the controlled low-intensity exercise bout, compared with WT mice, LFABP$^{-/-}$ mice utilized relatively more carbohydrate for energy production in the beginning of the exercise, reflected by the higher RER and increased glycogenolysis. Later on, LFABP$^{-/-}$ mice switched to use more lipids as an energy source, with a lower RER and elevated plasma FFA, likely from lipolysis in adipose tissue. Moreover, although gluconeogenesis may be limited by substrate levels in LFABP$^{-/-}$ mice at rest, their higher gluconeogenesis capacity may contribute to better energy production during exercise, with elevated gluconeogenic precursors in circulation (57, 58) and, particularly, more glycerol released from adipose tissue along with FFA in LFABP$^{-/-}$ mice. Overall, consistent with their higher aerobic exercise capacity, LFABP$^{-/-}$ mice seem to rely more on FA oxidation for energy production during a controlled treadmill test, suggesting that the exercise for LFABP$^{-/-}$ mice may be at a relatively lower intensity compared with WT mice.

In summary, LFABP ablation in the liver and intestine prevents the high-fat feeding–induced decline in exercise capacity, with metabolic reprogramming in the skeletal muscle including improved mitochondrial function and increased storage of muscle glycogen and IMTG. As LFABP is the only FABP highly expressed in the liver, we propose that the lack of LFABP, which diminishes hepatic lipid-handling capacity (12, 48), shunts surplus FA into circulation and to other peripheral tissues, including white adipose tissue and skeletal muscle. In the resting state, the restricted mitochondrial FA import in LFABP$^{-/-}$ muscle protects the mitochondria from sustained lipid overload and thereby preserves mitochondrial function and aerobic exercise capacity. This restriction in basal mitochondrial FA import does not seem to affect exercise-induced FA oxidation, as LFABP$^{-/-}$ mice preferentially utilized plasma FFA as their fuel source during a low-intensity exercise compared with WT, in keeping with their higher exercise capacity. With similar expression levels of the muscle FABP (*fabp3*) and insulin sensitivity, the metabolic alterations in the skeletal muscle underlying the exercise phenotype of LFABP$^{-/-}$ mice are likely the results of insulin-independent interorgan signaling that has yet to be identified. Our report provides a model of obesity with unimpaired physical fitness, and the findings on the muscle metabolic profile in the LFABP$^{-/-}$ mouse could have important implications for identifying therapeutic targets to counter obesity and metabolic syndrome by improving exercise capacity.

Experimental procedures

Animal and diets

LFABP$^{-/-}$ mice on a C57BL/6N background were generously provided by Binas and co-workers (59). The mice were back-crossed with WT C57BL/6J mice from The Jackson Laboratory (Bar Harbor, ME) to generate congenic C57BL/6 LFABP$^{-/-}$ mice of mixed J/N background (24); these were fur-

ther back-crossed six times to obtain LFABP$^{-/-}$ that are >98% J background. WT C57BL/6J mice obtained from The Jackson Laboratory and bred in our facility were used as controls; no differences were observed between these WT mice and littermate WT mice. Mice were maintained on a 12-h light/dark cycle and allowed *ad libitum* access to standard rodent chow (Purina Laboratory Rodent Diet 5015). At 2 months of age, male LFABP$^{-/-}$ and WT (C57BL/6J) mice were housed two to three per cage and fed a high-saturated-fat (45 kcal %) diet (HFS; Research Diets, Inc., D10080402) for 12 weeks. A low-fat diet containing 10 kcal % fat (LFD; Research Diets, Inc., D10080401) was also used for the initial evaluation of exercise capacity. Diet composition was detailed previously (18). Glycerol tolerance tests were performed on mice at 11 weeks of high-fat feeding. Following 16-h fasting and an intraperitoneal injection with glycerol (2 g/kg of body weight), blood glucose was measured before and within 3 h after the injection every 30 min with AlphaTRAK 2 blood glucose test strips (60). For primary myoblast isolation, male WT and LFABP$^{-/-}$ mice were fed HFS for 5 weeks starting at 4–5 weeks of age to improve myogenic yield and purity. At the end of the high-fat/low-fat feeding period, mice were euthanized by cervical dislocation prior to collection of blood and tissues. Rutgers University Animal Care and Use Committee approved all animal experiments.

Treadmill test for exercise capacity

After 12 weeks of high-fat feeding, mice were acclimatized to a motorized, speed-controlled treadmill with an electric shock stimulus (six lanes; Columbus Instruments, Columbus, OH) 1 day prior to the test day, running for 5 min at 6 m/min with 0° incline. On the test day, mice in the fed state were run on the treadmill with a speed increased from 6 m/min by 3 m/min every 3 min and a constant 25° incline. Another groups of mice were fasted for 16 h and run on the treadmill with a speed increased from 6 m/min by 3 m/min every 5 min and a 10° incline. The mice were run until they reached exhaustion, defined as when the mice remained on the shock grid for more than 5 s.

Energy expenditure during exercise

Energy expenditure during a low-intensity exercise bout was assessed using the Oxymax system (Columbus Instruments). At the end of 12 weeks of high-fat feeding, mice were acclimatized to the treadmill as described above. On the test day, the mice were fasted for 16 h, and each mouse was run individually on a treadmill positioned inside an indirect calorimetry chamber with rotating genotypes to minimize the effect of fasting time. The treadmill was set to a constant 10° incline throughout the test, and after 1-min settlement on a stationary treadmill and a 5-min warm-up at 5 m/min, the mice were run for 20 min at 10 m/min. Gas exchange and energy expenditure measurements were taken, with RER determined as VCO_2/VO_2, and energy expenditure calculated by $(3.815 + 1.232 \times RER) \times VO_2$ (61).

Preparation of tissue and plasma

For pre-exercise (resting) state studies, mice were fasted for 16 h before sacrifice at the end of the high-fat feeding period. For postexercise-state studies, mice were fasted for 16 h and sacrificed right after the low-intensity exercise bout. At sacrifice, blood was drawn, and glucose was measured with AlphaTRAK 2 blood glucose test strips. Plasma was extracted after centrifugation at 4 °C for 6 min at 3000 × *g* (~6000 rpm) and stored at −80 °C for further analysis. After the blood was taken, liver, epididymal white adipose tissue, and hind limb muscles (gastrocnemius, soleus, and quadriceps) were removed and immediately processed for same-day assays or placed on dry ice and subsequently stored at −80 °C for further analysis. For histochemical analyses, gastrocnemius muscle was removed, covered with optimum cutting temperature (OCT) compound, and flash frozen in liquid nitrogen–cooled isopentane for cryosectioning.

Insulin signaling

Mice were fasted for 4 h before the experiment. Before sacrifice, mice were intraperitoneally injected with PBS or insulin (Novolin R, Novo Nordisk) at a dose of 2 units/kg of body weight. Ten minutes later, gastrocnemius muscles were collected for protein extractions and Western blotting of phospho- and total AKT.

Plasma free fatty acid analysis

A plasma nonesterified fatty acid (NEFA) kit (Sigma, MAK044) was used to measure free fatty acid levels in plasma of postexercise mice.

Lipid extraction and triglyceride assay

Upon sacrifice, hind limb muscles were diluted with 8× the weight of the samples of PBS (pH 7.4)/g (wet weight) and homogenized for 2 min with a Potter–Elvehjem homogenizer on ice. Protein concentration was determined using the Bradford assay (24), and lipid extraction was performed on samples containing 1 mg of protein/ml using the Folch procedure (62). Lipids were extracted twice with 10 ml of chloroform/methanol (2:1), and the aqueous-phase nonlipid fractions were discarded. The organic lipid layer was dried under a nitrogen stream, resuspended in chloroform/methanol (1:1), and spotted onto Silica Gel G TLC plates along with authentic standards. The TLC plate was developed in a nonpolar solvent system consisting of hexane/diethyl ether/acetic acid (70:30:1), visualized by iodine staining, and scanned with a Hewlett–Packard scanner. Absolute values for triglyceride mass were obtained by densitometric analysis with ImageJ software based on the standard curves using authentic standards.

Glycogen assay

Total glycogen content in hind limb muscles was measured as described by Xu *et al.* (64) with minor modification (63). Briefly, hind limb muscles were homogenized with a Polytron for 1 min on ice in 5× the weight of the samples of PBS (pH 7.4)/g (wet weight) and centrifuged at 18,000 × *g* (~14,000 rpm) for 5 min after heat inactivation at 80 °C for 10 min. 20 μl of supernatant or standard solutions were mixed with amyloglucosidase (Sigma, A1602-25MG) to hydrolyze glycogen to glucose, and the glucose levels were measured colorimetrically with a glucose assay kit (Sigma, GAGO-20). Glycogen (Sigma,

G0885-1G) standard was used to plot a standard curve and determine the amount of glucose broken down from glycogen in the homogenate.

Mitochondrial enzyme assays

Mitochondrial enzymatic activities for CS, CCOX, and SDH were measured in fresh muscle homogenates as described (65, 66). Briefly, on the day of sacrifice, hind limb muscles were homogenized with a Potter–Elvehjem homogenizer for 2 min on ice in 20× the weight of the samples of Tris–sucrose buffer (20 mM Tris, 100 mM KCl, 70 mM sucrose, 1 mM EGTA, pH 7.4)/g (wet weight) and centrifuged at 600 × *g* for 10 min at 4 °C. Supernatant was collected, flash frozen in liquid nitrogen, and stored at −80 °C. Protein concentration in the supernatant was determined by Bradford assay (24). All enzyme assays were performed within linear ranges for protein concentration and reaction time.

CS activity was determined by measuring the formation of thionitrobenzoate anion. Muscle homogenates were mixed with 200 mM Tris (pH 8.0) with 0.2% Triton X-100 (v/v), 1 mM dithionitrobenzoic acid, and 10 mM acetyl-CoA. The reaction was started by adding 9.0 mM oxaloacetate, and absorbance was read at 412 nm every 30 s for 3 min.

SDH activity was determined by the rate of reduction of coenzyme Q1 (ubiquinone). Muscle homogenates were incubated with 0.5 M KP_i (pH 7.4) containing 0.01 M succinate for 10 min at 37 °C to activate complex II. Rotenone and antimycin A were added, and baseline absorbance was recorded. The reaction was started by adding 5 μl of coenzyme Q1, and the absorbance was recorded at 280 nm over 2 min.

CCOX activity was determined by measuring the rate of oxidation of cytochrome *c*. Reduced cytochrome *c* was freshly prepared by addition of sodium dithionite and added to 100 mM KP_i buffer (pH 7.4). Baseline absorbance at 550 nm was recorded for 2 min. Muscle homogenates were added to the mixture to start the reaction, and the absorbance at 550 nm was recorded for 3 min.

Fatty acid oxidation

Fatty acid oxidation rates in skeletal muscle homogenates were measured as detailed by Hirschey and co-workers (67, 68). Briefly, upon sacrifice, hind limb muscles were gently homogenized with a Potter–Elvehjem homogenizer for 15 strokes on ice in 6.5× the weight of the samples of sucrose–Tris–EDTA buffer/g (wet weight), and the homogenates were incubated for 30 min with 400 μl of reaction mixture containing 0.8 μCi of [^{14}C]oleate solubilized in 0.7% bovine serum albumin (BSA), 500 μM palmitate. $^{14}CO_2$ generated from the reaction was released by addition of 200 μl of perchloric acid and absorbed onto a piece of filter paper in the tube cap soaked with 20 μl of 1 M benzethonium hydroxide. The filter paper and ^{14}C-labeled ASMs in the reaction mixture were assessed for radioactivity by scintillation counting.

Cellular bioenergetics analysis

Primary myoblasts were isolated from gastrocnemius muscles of high fat–fed WT and LFABP$^{-/-}$ mice as described (70, 71). After eliminating fibroblasts using the preplating techniques, primary myoblasts were seeded (60,000 cells/well; triplicates) on collagen I– coated XF24 microplates (Seahorse Bioscience) and incubated at 37 °C overnight in F-10 Nutrient Mix (Thermo Fisher Scientific) supplemented with 10% fetal bovine Serum (Thermo Fisher Scientific), 10 ng/ml human fibroblast growth factor (PeproTech), and 1% penicillin-streptomycin (Thermo Fisher Scientific). Before the mitochondrial function analysis, myoblasts were incubated in Seahorse XF Assay Medium (Agilent, Seahorse Bioscience, 102353-100) supplemented with sodium pyruvate, L-glutamine, and glucose for 1 h. Using the mitochondrial stress test procedure with the Seahorse XFe24 system, the oxygen consumption rate and extracellular acidification rate were first determined under basal conditions. Through the multiport drug injection system, ATP production, maximal respiration, and nonmitochondrial respiration levels were determined in response to 1 μM oligomycin (VWR), 2 μM trifluoromethoxy carbonyl cyanide phenylhydrazone (FCCP) (Cayman Chemicals), and 0.5 μM rotenone + antimycin A (Sigma), respectively.

Quantitative RT-PCR for mRNA expression analysis

Total RNA was extracted from frozen muscles (TRIzol, Invitrogen) and further purified using RNeasy cleanup kits along with DNase treatment to minimize genomic DNA contamination (Qiagen). cDNA was synthesized using a reverse transcription kit (Invitrogen). Primer sequences were retrieved from Primer Bank (Harvard Medical School QPCR primer database) and are shown in Table S1. Efficiency tests were performed for all primers to confirm similar amplification efficiency (100 ± 10%) between the genotypes. Real-time PCRs were performed in triplicate using an Applied Biosystems StepOne Plus instrument. Each reaction contained 100 ng of cDNA, 250 nM each primer, and 12.5 μl of Power SYBR Green Master Mix (Thermo Fisher) in a total volume of 25 μl. Relative expression of the target genes was calculated using the comparative Ct method and normalized to endogenous β-actin.

Western blotting for protein analysis

Gastrocnemius muscles were homogenized in 12 volumes of radioimmune precipitation assay buffer (Cell Signaling Technology, 9806) with protease and phosphatase inhibitor (Thermo Fisher, A32961) with a Potter–Elvehjem homogenizer for 2 min on ice. The homogenates were centrifuged at 20,000 × *g* (~15,000 rpm) at 4 °C for 20 min to separate the supernatant as total protein extracts, plasma membrane or mitochondrial fraction was prepared by sequential centrifugation as described (72, 73), and the protein concentration was determined by Bradford assay (24). Equal amounts of protein, as indicated, were resolved by SDS-PAGE and transferred onto nitrocellulose membranes using a wet transfer system (Bio-Rad) at 20 V overnight at 4 °C. The membranes were blocked in 5% (w/v) BSA solution for 1 h at room temperature. For total protein extracts, the membranes were probed with phospho-AKT, AKT, GAPDH (1:1000; Cell Signaling Technology, 4060, 2920, and 2118, respectively), MHC 1, MHC 2a, and MHC 2b antibodies (1:100; Developmental Studies Hybridoma Bank, BA-F8, SC-71, and 10F5, respectively) at 4 °C overnight. For the plasma membrane

fraction, the membranes were probed with GLUT4 and insulin receptor β (1:500; Cell Signaling Technology, 2213 and 3025, respectively). For the mitochondrial fraction, the membranes were probed with oxidative phosphorylation (OXPHOS) antibody mixture (1:250; Abcam, ab110413) and VDAC1 antibody (1:1000; Abcam, ab15895). Primary antibody incubation was followed by IRDye® 800CW and 680RD secondary antibodies (LI-COR Biosciences) for 1 h, and detection was done using the 800 channel of the Odyssey® Imaging System (LI-COR Biosciences).

Histochemical analyses

Frozen sections (10 μm) were cut in a cryostat, placed on microscope slides, and stored at −80 °C for further analysis. On the staining day, slides were allowed to come to room temperature and then fixed in 4% paraformaldehyde, PBS. Intramuscular triglyceride was stained with a solution of triethyl phosphate saturated with oil red O (Sigma, O0625) as described (74). Oil red O stained–sections were examined in brightfield and epifluorescence using a Texas Red excitation filter (540–580 nm).

Metabolomics

Metabolomics analysis of frozen livers, plasma, and gastrocnemius muscles from WT and LFABP$^{-/-}$ mice was performed by Metabolon (Durham, NC) ($n = 5$ per group for livers and plasma, $n = 6$ per group for muscles). Nontargeted metabolic profiling was conducted using three independent platforms: ultrahigh-performance LC/tandem MS (LC/MS) optimized for basic species, LC/MS optimized for acidic species, and GC/MS as described previously (7, 75). Metabolites were identified by automated matching to chemical reference library standards on the basis of retention time, molecular weight (m/z), preferred adducts, and in-source fragments as well as associated MS spectra and curated using software developed at Metabolon (69). Following log transformation and imputation of missing values with minimum observed values, statistical tests (*e.g.* *t* tests, ANOVA with contrasts, etc.) were used to identify biochemicals that differ significantly between experimental groups. An estimate of the false discovery rate (q value) was also calculated to take into account the multiple comparisons in metabolomic analysis.

Statistics

Data represent mean ± S.E. Statistical comparisons were made by two-tailed Student's *t* test (LFABP$^{-/-}$ *versus* WT). A p value of less than 0.05 was considered statistically significant. The effect of genotype (substrain) was compared by one-way ANOVA followed by Tukey's post hoc test.

Author contributions—H. X., A. M. G., G. C. H., and J. S. conceptualization; H. X. and J. S. data curation; H. X. formal analysis; H. X. validation; H. X., A. M. G., Y. X. Z., C. P., Z. S., and A. F. investigation; H. X. visualization; H. X., A. M. G., Y. X. Z., G. C. H., and J. S. methodology; H. X. writing-original draft; H. X. and J. S. writing-review and editing; J. S. resources; J. S. software; J. S. supervision; J. S. funding acquisition; J. S. project administration.

Acknowledgments—We thank Dr. Malcolm Watford, Dr. Tracy Anthony, Dr. Harini Sampath, and Dr. Rosalind Coleman for helpful suggestions during this work; Dr. Michael Verzi and Dr. Lei Chen for helping with cryosectioning and histochemistry; and Dr. David Cohen and Dr. Norihiro Imai for expert advice on primary myoblasts isolation.

References

1. Savage, D. B., Petersen, K. F., and Shulman, G. I. (2007) Disordered lipid metabolism and the pathogenesis of insulin resistance. *Physiol. Rev.* **87,** 507–520 CrossRef Medline
2. Unger, R. H. (2003) Minireview: weapons of lean body mass destruction: the role of ectopic lipids in the metabolic syndrome. *Endocrinology* **144,** 5159–5165 CrossRef Medline
3. Chmurzyńska, A. (2006) The multigene family of fatty acid-binding proteins (FABPs): function, structure and polymorphism. *J. Appl. Genet.* **47,** 39–48 CrossRef Medline
4. Thompson, J., Winter, N., Terwey, D., Bratt, J., and Banaszak, L. (1997) The crystal structure of the liver fatty acid-binding protein. A complex with two bound oleates. *J. Biol. Chem.* **272,** 7140–7150 CrossRef Medline
5. Wolfrum, C., Borrmann, C. M., Borchers, T., and Spener, F. (2001) Fatty acids and hypolipidemic drugs regulate peroxisome proliferator-activated receptors α-and γ-mediated gene expression via liver fatty acid binding protein: a signaling path to the nucleus. *Proc. Natl. Acad. Sci. U.S.A.* **98,** 2323–2328 CrossRef Medline
6. Lagakos, W. S., Guan, X., Ho, S.-Y., Sawicki, L. R., Corsico, B., Kodukula, S., Murota, K., Stark, R. E., and Storch, J. (2013) Liver fatty acid-binding protein binds monoacylglycerol *in vitro* and in mouse liver cytosol. *J. Biol. Chem.* **288,** 19805–19815 CrossRef Medline
7. Boudonck, K. J., Mitchell, M. W., Német, L., Keresztes, L., Nyska, A., Shinar, D., and Rosenstock, M. (2009) Discovery of metabolomics biomarkers for early detection of nephrotoxicity. *Toxicol. Pathol.* **37,** 280–292 CrossRef Medline
8. Wolfrum, C., Buhlmann, C., Rolf, B., Börchers, T., and Spener, F. (1999) Variation of liver-type fatty acid binding protein content in the human hepatoma cell line HepG2 by peroxisome proliferators and antisense RNA affects the rate of fatty acid uptake. *Biochim. Biophys. Acta* **1437,** 194–201 CrossRef Medline
9. Hostetler, H. A., McIntosh, A. L., Atshaves, B. P., Storey, S. M., Payne, H. R., Kier, A. B., and Schroeder, F. (2009) L-FABP directly interacts with PPARα in cultured primary hepatocytes. *J. Lipid Res.* **50,** 1663–1675 CrossRef Medline
10. Kersten, S., Desvergne, B., and Wahli, W. (2000) Roles of PPARs in health and disease. *Nature* **405,** 421–424 CrossRef Medline
11. Francis, G. A., Fayard, E., Picard, F., and Auwerx, J. (2003) Nuclear receptors and the control of metabolism. *Annu. Rev. Physiol.* **65,** 261–311 CrossRef Medline
12. Martin, G. G., Huang, H., Atshaves, B. P., Binas, B., and Schroeder, F. (2003) Ablation of the liver fatty acid binding protein gene decreases fatty acyl CoA binding capacity and alters fatty acyl CoA pool distribution in mouse liver. *Biochemistry* **42,** 11520–11532 CrossRef Medline
13. Newberry, E. P., Xie, Y., Kennedy, S., Han, X., Buhman, K. K., Luo, J., Gross, R. W., and Davidson, N. O. (2003) Decreased hepatic triglyceride accumulation and altered fatty acid uptake in mice with deletion of the liver fatty acid-binding protein gene. *J. Biol. Chem.* **278,** 51664–51672 CrossRef Medline
14. Erol, E., Kumar, L. S., Cline, G. W., Shulman, G. I., Kelly, D. P., and Binas, B. (2004) Liver fatty acid binding protein is required for high rates of hepatic fatty acid oxidation but not for the action of PPARα in fasting mice. *FASEB J.* **18,** 347–349 CrossRef Medline
15. Haunerland, N. H., and Spener, F. (2004) Fatty acid-binding proteins—insights from genetic manipulations. *Prog. Lipid Res.* **43,** 328–349 CrossRef Medline
16. Martin, G. G., Atshaves, B. P., McIntosh, A. L., Mackie, J. T., Kier, A. B., and Schroeder, F. (2005) Liver fatty-acid-binding protein (L-FABP) gene

ablation alters liver bile acid metabolism in male mice. *Biochem. J.* **391,** 549–560 CrossRef Medline
17. Martin, G. G., Atshaves, B. P., McIntosh, A. L., Mackie, J. T., Kier, A. B., and Schroeder, F. (2006) Liver fatty acid binding protein gene ablation potentiates hepatic cholesterol accumulation in cholesterol-fed female mice. *Am. J. Physiol. Gastrointest. Liver Physiol.* **290,** G36–G48 CrossRef Medline
18. Gajda, A. M., Zhou, Y. X., Agellon, L. B., Fried, S. K., Kodukula, S., Fortson, W., Patel, K., and Storch, J. (2013) Direct comparison of mice null for liver or intestinal fatty acid-binding proteins reveals highly divergent phenotypic responses to high fat feeding. *J. Biol. Chem.* **288,** 30330–30344 CrossRef Medline
19. Atshaves, B. P., McIntosh, A. L., Storey, S. M., Landrock, K. K., Kier, A. B., and Schroeder, F. (2010) High dietary fat exacerbates weight gain and obesity in female liver fatty acid binding protein gene-ablated mice. *Lipids* **45,** 97–110 CrossRef Medline
20. Newberry, E. P., Xie, Y., Kennedy, S. M., Luo, J., and Davidson, N. O. (2006) Protection against Western diet–induced obesity and hepatic steatosis in liver fatty acid–binding protein knockout mice. *Hepatology* **44,** 1191–1205 CrossRef Medline
21. Salvadori, A., Fanari, P., Fontana, M., Buontempi, L., Saezza, A., Baudo, S., Miserocchi, G., and Longhini, E. (1999) Oxygen uptake and cardiac performance in obese and normal subjects during exercise. *Respiration* **66,** 25–33 CrossRef Medline
22. Regensteiner, J. G., Sippel, J., McFarling, E. T., Wolfel, E. E., and Hiatt, W. R. (1995) Effects of non-insulin-dependent diabetes on oxygen consumption during treadmill exercise. *Med. Sci. Sports Exerc.* **27,** 661–667 Medline
23. Newberry, E. P., Kennedy, S. M., Xie, Y., Luo, J., and Davidson, N. O. (2009) Diet-induced alterations in intestinal and extrahepatic lipid metabolism in liver fatty acid binding protein knockout mice. *Mol. Cell. Biochem.* **326,** 79–86 CrossRef Medline
24. Lagakos, W. S., Gajda, A. M., Agellon, L., Binas, B., Choi, V., Mandap, B., Russnak, T., Zhou, Y. X., and Storch, J. (2011) Different functions of intestinal and liver-type fatty acid-binding proteins in intestine and in whole body energy homeostasis. *Am. J. Physiol. Gastrointest. Liver Physiol.* **300,** G803–G814 CrossRef Medline
25. Xu, H., Gajda, A., Zhou, Y. X., Fatima, A., and Storch, J. (2017) Energy substrate levels and metabolic changes in skeletal muscle underlie increased activity and improved exercise performance in liver fatty acid-binding protein null mice. *FASEB J.* **31,** (suppl.) Abstr. 782.10
26. Kravitz, L., and Dalleck, L. C. (2002) Physiological factors limiting endurance exercise capacity, in *Advanced Sports Conditioning for Enhanced Performance. IDEA Resource Series*, pp. 21–27, IDEA Health & Fitness Association, San Diego, CA
27. Koves, T. R., Ussher, J. R., Noland, R. C., Slentz, D., Mosedale, M., Ilkayeva, O., Bain, J., Stevens, R., Dyck, J. R., Newgard, C. B., Lopaschuk, G. D., and Muoio, D. M. (2008) Mitochondrial overload and incomplete fatty acid oxidation contribute to skeletal muscle insulin resistance. *Cell Metab.* **7,** 45–56 CrossRef Medline
28. Costill, D. L. (1970) Metabolic responses during distance running. *J. Appl. Physiol.* **28,** 251–255 CrossRef Medline
29. Bassett, D. R, Jr., and Howley, E. T. (2000) Limiting factors for maximum oxygen uptake and determinants of endurance performance. *Med. Sci. Sports Exerc.* **32,** 70–84 Medline
30. Gabriel, B. M., and Zierath, J. R. (2017) The limits of exercise physiology: from performance to health. *Cell metabolism* **25,** 1000–1011 CrossRef Medline
31. Lee-Young, R. S., Ayala, J. E., Fueger, P. T., Mayes, W. H., Kang, L., and Wasserman, D. H. (2011) Obesity impairs skeletal muscle AMPK signaling during exercise: role of AMPKα2 in the regulation of exercise capacity *in vivo*. *Int. J. Obes.* **35,** 982–989 CrossRef Medline
32. Yokota, T., Kinugawa, S., Hirabayashi, K., Matsushima, S., Inoue, N., Ohta, Y., Hamaguchi, S., Sobirin, M. A., Ono, T., Suga, T., Kuroda, S., Tanaka, S., Terasaki, F., Okita, K., and Tsutsui, H. (2009) Oxidative stress in skeletal muscle impairs mitochondrial respiration and limits exercise capacity in type 2 diabetic mice. *Am. J. Physiol. Heart Circ. Physiol.* **297,** H1069–H1077 CrossRef Medline
33. Petersen, K. F., Dufour, S., Savage, D. B., Bilz, S., Solomon, G., Yonemitsu, S., Cline, G. W., Befroy, D., Zemany, L., Kahn, B. B., Papademetris, X., Rothman, D. L., and Shulman, G. I. (2007) The role of skeletal muscle insulin resistance in the pathogenesis of the metabolic syndrome. *Proc. Natl. Acad. Sci. U.S.A.* **104,** 12587–12594 CrossRef Medline
34. Murray, A. J., Knight, N. S., Cochlin, L. E., McAleese, S., Deacon, R. M., Rawlins, J. N., and Clarke, K. (2009) Deterioration of physical performance and cognitive function in rats with short-term high-fat feeding. *FASEB J.* **23,** 4353–4360 CrossRef Medline
35. Xiao, Y., Wang, W., Chen, L., Chen, J., Jiang, P., Fu, X., Nie, X., Kwan, H., Liu, Y., and Zhao, X. (2017) The effects of short-term high-fat feeding on exercise capacity: multi-tissue transcriptome changes by RNA sequencing analysis. *Lipids Health Dis.* **16,** 28 CrossRef Medline
36. Borghouts, L. B., and Keizer, H. A. (2000) Exercise and insulin sensitivity: a review. *Int. J. Sports Med.* **21,** 1–12 CrossRef Medline
37. Hawley, J. A. (2004) Exercise as a therapeutic intervention for the prevention and treatment of insulin resistance. *Diabetes Metab. Res. Rev.* **20,** 383–393 CrossRef Medline
38. Blair, S. N., and Brodney, S. (1999) Effects of physical inactivity and obesity on morbidity and mortality: current evidence and research issues. *Med. Sci. Sports Exerc.* **31,** S646–S662 CrossRef Medline
39. Wei, M., Gibbons, L. W., Kampert, J. B., Nichaman, M. Z., and Blair, S. N. (2000) Low cardiorespiratory fitness and physical inactivity as predictors of mortality in men with type 2 diabetes. *Ann. Int. Med.* **132,** 605–611 CrossRef Medline
40. Phillips, C. M. (2013) Metabolically healthy obesity: definitions, determinants and clinical implications. *Rev. Endocr. Metab. Disord.* **14,** 219–227 CrossRef Medline
41. Blüher, M. (2014) Are metabolically healthy obese individuals really healthy? *Eur. J. Endocrinol.* **171,** R209–R219 CrossRef Medline
42. Stefan, N., Häring, H.-U., Hu, F. B., and Schulze, M. B. (2013) Metabolically healthy obesity: epidemiology, mechanisms, and clinical implications. *Lancet Diabetes Endocrinol.* **1,** 152–162 CrossRef Medline
43. Appleton, S. L., Seaborn, C. J., Visvanathan, R., Hill, C. L., Gill, T. K., Taylor, A. W., Adams, R. J., and North West Adelaide Health Study Team (2013) Diabetes and cardiovascular disease outcomes in the metabolically healthy obese phenotype: a cohort study. *Diabetes Care* **36,** 2388–2394 CrossRef Medline
44. Soriguer, F., Gutiérrez-Repiso, C., Rubio-Martín, E., García-Fuentes, E., Almaraz, M. C., Colomo, N., Esteva de Antonio, I., de Adana, M. S. R., Chaves, F. J., and Morcillo, S. (2013) Metabolically healthy but obese, a matter of time? Findings from the prospective Pizarra study. *J. Clin. Endocrinol. Metab.* **98,** 2318–2325 CrossRef Medline
45. Jung, C. H., Lee, W. J., and Song, K.-H. (2017) Metabolically healthy obesity: a friend or foe? *Korean J. Int. Med.* **32,** 611–621 CrossRef Medline
46. Ebeling, P., Koistinen, H. A., and Koivisto, V. A. (1998) Insulin-independent glucose transport regulates insulin sensitivity. *FEBS Lett.* **436,** 301–303 CrossRef Medline
47. Eaton, S. (2002) Control of mitochondrial β-oxidation flux. *Prog. Lipid Res.* **41,** 197–239 CrossRef Medline
48. Martin, G. G., Atshaves, B. P., Huang, H., McIntosh, A. L., Williams, B. J., Pai, P.-J., Russell, D. H., Kier, A. B., and Schroeder, F. (2009) Hepatic phenotype of liver fatty acid binding protein gene-ablated mice. *Am. J. Physiol. Gastrointest. Liver Physiol.* **297,** G1053–G1065 CrossRef Medline
49. Martins, A. R., Nachbar, R. T., Gorjao, R., Vinolo, M. A., Festuccia, W. T., Lambertucci, R. H., Cury-Boaventura, M. F., Silveira, L. R., Curi, R., and Hirabara, S. M. (2012) Mechanisms underlying skeletal muscle insulin resistance induced by fatty acids: importance of the mitochondrial function. *Lipids Health Dis.* **11,** 30 CrossRef Medline
50. Finck, B. N., Bernal-Mizrachi, C., Han, D. H., Coleman, T., Sambandam, N., LaRiviere, L. L., Holloszy, J. O., Semenkovich, C. F., and Kelly, D. P. (2005) A potential link between muscle peroxisome proliferator-activated receptor-α signaling and obesity-related diabetes. *Cell Metab.* **1,** 133–144 CrossRef Medline
51. Guerre-Millo, M., Rouault, C., Poulain, P., André, J., Poitout, V., Peters, J. M., Gonzalez, F. J., Fruchart, J.-C., Reach, G., and Staels, B. (2001) PPAR-α–null mice are protected from high-fat diet–induced insulin resistance. *Diabetes* **50,** 2809–2814 CrossRef Medline

52. Bouzakri, K., Austin, R., Rune, A., Lassman, M. E., Garcia-Roves, P. M., Berger, J. P., Krook, A., Chibalin, A. V., Zhang, B. B., and Zierath, J. R. (2008) Malonyl coenzymeA decarboxylase regulates lipid and glucose metabolism in human skeletal muscle. *Diabetes* **57,** 1508–1516 CrossRef Medline
53. Choi, C. S., Befroy, D. E., Codella, R., Kim, S., Reznick, R. M., Hwang, Y.-J., Liu, Z.-X., Lee, H.-Y., Distefano, A., Samuel, V. T., Zhang, D., Cline, G. W., Handschin, C., Lin, J., Petersen, K. F., Spiegelman, B. M., and Shulman, G. I. (2008) Paradoxical effects of increased expression of PGC-1α on muscle mitochondrial function and insulin-stimulated muscle glucose metabolism. *Proc. Natl. Acad. Sci. U.S.A.* **105,** 19926–19931 CrossRef Medline
54. Montgomery, M. K., and Turner, N. (2015) Mitochondrial dysfunction and insulin resistance: an update. *Endocr. Connect.* **4,** R1–R15 CrossRef Medline
55. Brooks, G. A., and Mercier, J. (1994) Balance of carbohydrate and lipid utilization during exercise: the "crossover" concept. *J. Appl. Physiol.* **76,** 2253–2261 CrossRef Medline
56. Romijn, J., Coyle, E., Sidossis, L., Gastaldelli, A., Horowitz, J., Endert, E., and Wolfe, R. (1993) Regulation of endogenous fat and carbohydrate metabolism in relation to exercise intensity and duration. *Am. J. Physiol. Endocrinol. Metab.* **265,** E380–E391 CrossRef Medline
57. Wasserman, D. H., Lacy, D. B., Bracy, D., and Williams, P. E. (1992) Metabolic regulation in peripheral tissues and transition to increased gluconeogenic mode during prolonged exercise. *Am. J. Physiol. Endocrinol. Metab.* **263,** E345–E354 CrossRef Medline
58. Lewis, G. D., Farrell, L., Wood, M. J., Martinovic, M., Arany, Z., Rowe, G. C., Souza, A., Cheng, S., McCabe, E. L., Yang, E., Shi, X., Deo, R., Roth, F. P., Asnani, A., Rhee, E. P., *et al*. (2010) Metabolic signatures of exercise in human plasma. *Sci. Transl. Med.* **2,** 33ra37 CrossRef Medline
59. Martin, G. G., Danneberg, H., Kumar, L. S., Atshaves, B. P., Erol, E., Bader, M., Schroeder, F., and Binas, B. (2003) Decreased liver fatty acid binding capacity and altered liver lipid distribution in mice lacking the liver fatty acid-binding protein gene. *J. Biol. Chem.* **278,** 21429–21438 CrossRef Medline
60. Leonardi, R., Rehg, J. E., Rock, C. O., and Jackowski, S. (2010) Pantothenate kinase 1 is required to support the metabolic transition from the fed to the fasted state. *PLoS One* **5,** e11107 CrossRef Medline
61. McLean, J., and Tobin, G. (1987) *Animal and Human Calorimetry*, pp. 30–32, Cambridge University Press, Cambridge, UK
62. Folch, J., Lees, M., and Sloane-Stanley, G. (1957) A simple method for the isolation and purification of total lipids from animal tissues. *J. Biol. Chem.* **226,** 497–509 Medline
63. Passonneau, J. V., and Lauderdale, V. R. (1974) A comparison of three methods of glycogen measurement in tissues. *Anal. Biochem.* **60,** 405–412 CrossRef Medline
64. Xu, K., Zheng, X., and Sehgal, A. (2008) Regulation of feeding and metabolism by neuronal and peripheral clocks in *Drosophila*. *Cell Metab.* **8,** 289–300 CrossRef Medline
65. Spinazzi, M., Casarin, A., Pertegato, V., Salviati, L., and Angelini, C. (2012) Assessment of mitochondrial respiratory chain enzymatic activities on tissues and cultured cells. *Nat. Protoc.* **7,** 1235–1246 CrossRef Medline
66. O'Neill, H. M., Maarbjerg, S. J., Crane, J. D., Jeppesen, J., Jørgensen, S. B., Schertzer, J. D., Shyroka, O., Kiens, B., van Denderen, B. J., Tarnopolsky, M. A., Kemp, B. E., Richter, E. A., and Steinberg, G. R. (2011) AMP-activated protein kinase (AMPK) $\beta1\beta2$ muscle null mice reveal an essential role for AMPK in maintaining mitochondrial content and glucose uptake during exercise. *Proc. Natl. Acad. Sci. U.S.A.* **108,** 16092–16097 CrossRef Medline
67. Hirschey, M. D., and Verdin, E. (2010) Measuring fatty acid oxidation in tissue homogenates. *Protocol Exchange* **10,** 1038 CrossRef
68. Huynh, F. K., Green, M. F., Koves, T. R., and Hirschey, M. D. (2014) Measurement of fatty acid oxidation rates in animal tissues and cell lines. *Methods Enzymol.* **542,** 391–405 CrossRef Medline
69. DeHaven, C. D., Evans, A. M., Dai, H., and Lawton, K. A. (2010) Organization of GC/MS and LC/MS metabolomics data into chemical libraries. *J. Cheminform.* **2,** 9 CrossRef Medline
70. Lavasani, M., Lu, A., Thompson, S. D., Robbins, P. D., Huard, J., and Niedernhofer, L. J. (2013) Isolation of muscle-derived stem/progenitor cells based on adhesion characteristics to collagen-coated surfaces. *Methods Mol. Biol.* **976,** 53–65 CrossRef Medline
71. Hindi, L., McMillan, J. D., Afroze, D., Hindi, S. M., and Kumar, A. (2017) Isolation, culturing, and differentiation of primary myoblasts from skeletal muscle of adult mice. *Bio Protoc.* **7,** e2248 CrossRef Medline
72. Nishiumi, S., and Ashida, H. (2007) Rapid preparation of a plasma membrane fraction from adipocytes and muscle cells: application to detection of translocated glucose transporter 4 on the plasma membrane. *Biosci. Biotechnol. Biochem.* **71,** 2343–2346 CrossRef Medline
73. Garcia-Cazarin, M. L., Snider, N. N., and Andrade, F. H. (2011) Mitochondrial isolation from skeletal muscle. *J. Vis. Exp.* 2452 CrossRef Medline
74. Koopman, R., Schaart, G., and Hesselink, M. K. (2001) Optimisation of oil red O staining permits combination with immunofluorescence and automated quantification of lipids. *Histochem. Cell Biol.* **116,** 63–68 Medline
75. Evans, A. M., DeHaven, C. D., Barrett, T., Mitchell, M., and Milgram, E. (2009) Integrated, nontargeted ultrahigh performance liquid chromatography/electrospray ionization tandem mass spectrometry platform for the identification and relative quantification of the small-molecule complement of biological systems. *Anal. Chem.* **81,** 6656–6667 CrossRef Medline